Computational Condensed Matter 23 (2020) e00453

Contents lists available at ScienceDirect

Computational Condensed Matter

journal homepage: http://ees.elsevier.com/cocom/default.asp

Orthorhombic $CsPbI_3$ perovskites: Thickness-dependent structural, optical and vibrational properties

S. Ozen [a], F. Iyikanat [b], M. Ozcan [a], G.E. Tekneci [c], I. Eren [b], Y. Sozen [a], H. Sahin [a, *]

[a] Department of Photonics, Izmir Institute of Technology, 35430, Izmir, Turkey
[b] Department of Physics, Izmir Institute of Technology, 35430, Izmir, Turkey
[c] Department of Materials Science and Engineering, Izmir Institute of Technology, 35430, Izmir, Turkey

ARTICLE INFO

Article history:
Received 22 October 2019
Received in revised form
24 December 2019
Accepted 25 December 2019

Keywords:
Density functional theory
Perovskites
Thickness dependency
Electronic band structure
Phonons
Optical properties

ABSTRACT

Cesium lead halide perovskites have been subject to intense investigation, mostly because of their potential to be used in optoelectronic device applications. However, regarding the need for nanoscale materials in forthcoming nanotechnology applications, understanding of how the characteristic properties of these perovskite crystals are modified through dimensional crossover is essential. In this study, thickness-dependence of the structural, electronic and vibrational properties of orthorhombic $CsPbI_3$, which is one of the most stable phase at room temperature, is investigated by means of state-of-the-art first-principles calculations. Our results show that (i) bilayers and monolayers of $CsPbI_3$ can be stabilized in orthorhombic crystal symmetry, (ii) among; the possible ultra-thin perovskites only structures with CsI-terminated surface are dynamically stable (iii) electronic band gap increases with decrease in perovskite thickness due to quantum size effect and (iv) reflectivity and transmissivity of the orthorhombic $CsPbI_3$ can be tuned by varying the thickness that modifies the electron confinement.

1. Introduction

In recent years, lead halide perovskites in the form of $APbX_3$ (where A: MA^+, FA^+, Cs^+, and X: Cl^+, Br^-, I^-) have attracted great attention thanks to their extraordinary optical properties such as long carrier lifetime, tunable wavelength, strong light absorption, and high photoluminescence quantum yield [1–7]. In order to tune their electronic properties and increase their stability, various methods such as anion exchange, doping, and dimensional modification have been carried out [8–13]. These properties and their tunability made perovskites suitable candidates for device applications such as lasers [14,15], solar cells [16,17], light emitting diodes [18–20], and photodetectors [21,22].

Apart from studies in perovskite nanocrystals, it has been shown that nanoscale materials may present unique characteristics due to the dimensional reduction. In the last two decades, discovery of graphene, has increased the interest in atomically thin two-dimensional (2D) materials that are suitable candidates for ultra-thin flexible optoelectronic devices [23]. Soon after, the studies on 2D materials such as hexagonal boron nitride (h-BN) [24], MoS_2 [25], transition metal dichalcogenides (TMDs) [26–29], and alkaline-earth-metal hydroxides (AEMHs) [30] indicated that reduction in number of layers from bulk to monolayer leads to significant changes in vibrational, optical and electrical properties. Following these advances, the interest in thickness dependent properties of organic, hybrid and $MAPbX_3$ perovskites which are suitable candidate for optoelectronic applications has started to increase and recent studies proved that also cesium lead halide perovskites' optical, electronic and vibrational properties may vary with their thickness [31–34].

Among cesium lead halide perovskites, cubic phase (α-$CsPbI_3$) show high thermal stability and excellent photoluminescence properties with a bandgap of 1.73 eV which is desirable for optoelectronic device applications [35,36]. Unfortunately, the phase transition is inevitable for α-$CsPbI_3$ perovskites which are stable at high temperature (>320 °C) [37] and at ambient conditions, the α-$CsPbI_3$ nanocrystals transform to the orthorhombic structure which is also called yellow-phase [35,38]. Although researches have been conducted the cubic $CsPbI_3$ to stabilize its structure, it has been found that the phase transition is inevitable and the orthorhombic phase is more favorable than the cubic phase at room temperature [39,40]. Therefore, understanding this phase is a key point for dealing with cesium lead halide perovskites. Theoretical

* Corresponding author.
E-mail address: hasansahin@iyte.edu.tr (H. Sahin).

https://doi.org/10.1016/j.cocom.2019.e00453
2352-2143/

studies showing the importance of optical and electronic properties of perovskite iodides have already been reported [41,42]. However, there are very few studies on how the characteristic properties of cesium perovskites are modified going from their bulk to ultra-thin structures [43,44].

In this study, motivated by recent advances in synthesis and characterization of Cs perovskites, we investigate dimensional reduction dependent structural, electrical, optical and vibrational characteristics of orthorhombic $CsPbI_3$ perovskite crystals. A detailed analysis, based on DFT simulations, for bulk and possible bilayer and single layer structures of $CsPbI_3$ are presented in detail.

This paper is organized as follows. Details of the computational methodology are given in Sec. II. DFT based investigations of structural, electronic and vibrational properties of bulk $CsPbI_3$ and effects of dimensional reduction from bulk to bilayer and monolayer are given in Sec. III and Sec. IV respectively. We conclude our results in Sec. V.

2. Computational methodology

Density functional theory-based calculations were performed using the projector augmented wave (PAW) [45,46] potentials as implemented in the Vienna ab initio Simulation Package (VASP) [47,48]. The exchange-correlation potentials are approximated by local density approximation (LDA) [49]. Bader technique was used to determine the charge transfer between the atoms [50].

A plane-wave basis set with kinetic energy cutoff of 500 eV was used for all the calculations. The total energy difference between the sequential steps in the iterations was taken to be 10^{-5} eV as the convergence criterion. The total force in the unit cell was reduced to a value less than 10^{-4} eV/Å Γ-centered k-point meshes of 4 × 4 x 3 and 4 × 4 x 1 were used for bulk and monolayer relaxations respectively and for the surface relaxations they were proportioned. For Pb- and Cs-terminated surfaces, vacuum spacing of 16 Å was incorporated to avoid interaction with neighboring surfaces. Gaussian smearing of 0.1 eV was used for bulk structures and 0.05 eV for single and bilayer structures electronic density of states calculations. The cohesive energy per atom was calculated using the formula

$$E_{coh} = \left[\sum_i n_{atom(i)} E_{atom(i)} - E_{system}\right] \Big/ n_{total} \quad (1)$$

where $E_{atom(i)}$ is isolated single atom energies for ith atom, while i stands for the number of all atoms for the same species, n_{total} represents the total number of atoms, and $n_{atom(i)}$ shows the numbers of same kind of atoms in the unit cell, respectively. In addition, we performed ab-initio molecular dynamic (MD) simulations to examine the stability of Cs_2PbI_4 monolayer stacked between two SnS_2 monolayers.

The frequency dependent dielectric function, $\varepsilon(\omega) = \varepsilon_1(\omega) + i\varepsilon_2(\omega)$, of the materials was calculated by using the PBE0 functional on top of SOC. Using the dielectric function, other optical spectral quantities such as the absorption coefficient (α), reflectivity (R), and transmissivity (T) were calculated with the following formulas;

$$\alpha(\omega) = \sqrt{2}\omega\left\{\left[\varepsilon_1(\omega)^2 + \varepsilon_2(\mathrm{w})^2\right]^{1/2} - \varepsilon_1(\omega)\right\}^{1/2} \quad (2)$$

$$\mathrm{R}(\omega) = \left|\frac{\sqrt{\varepsilon(\mathrm{w})} - 1}{\sqrt{\varepsilon(\omega)} + 1}\right|^2 \quad (3)$$

$$T(\omega) = (1 - R(\omega))^2 e^{-\alpha(\omega)l} \quad (4)$$

where l is the thickness of the material.

3. Possible structures of ultra-thin orthorhombic CsPbI3

This section is devoted to investigation of the possible ultra-thin crystal structures of orthorhombic $CsPbI_3$ structure which is the frequently obtained product at room temperature [51,52]. Crystal structures of the bulk and possible forms of bilayer and monolayer $CsPbI_3$ are shown in Fig. 1.

Total energy optimization calculations reveal that optimized lattice parameters of bulk orthorhombic $CsPbI_3$ crystal are $a = 7.93$ Å, $b = 8.94$ Å, and $c = 12.21$ Å. As seen in the figure, $CsPbI_3$

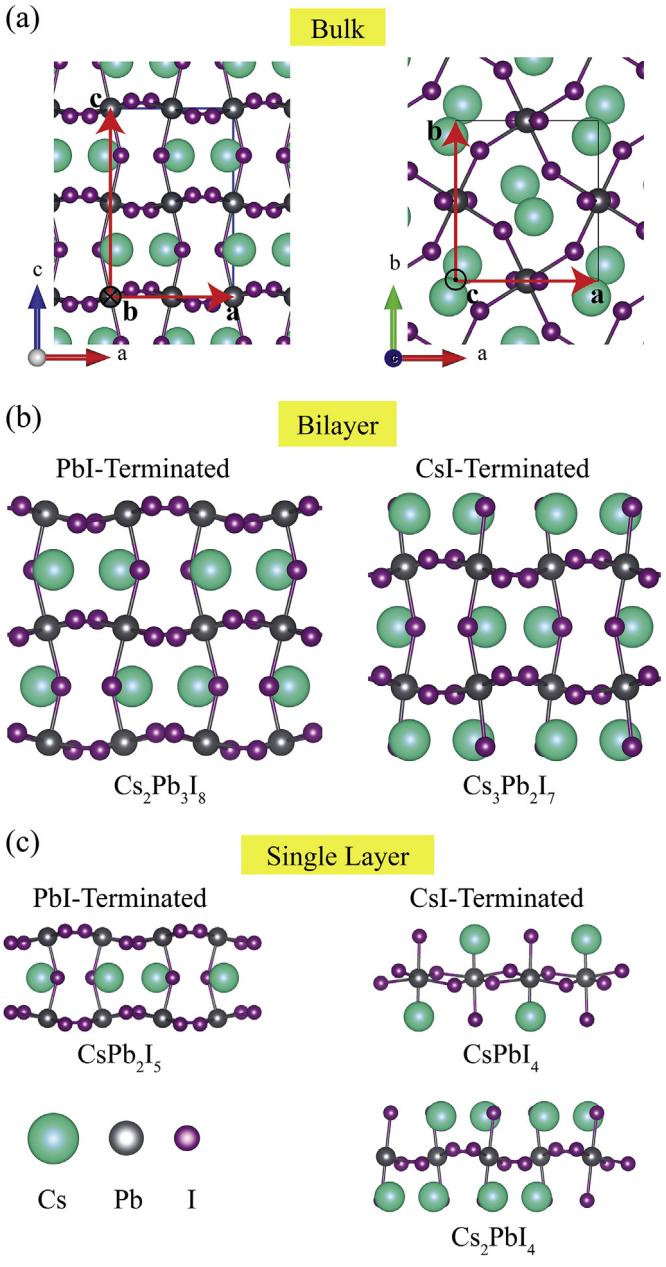

Fig. 1. (a) Bulk, (b) bilayer, (c) monolayer structures of $CsPbI_3$ crystal.

crystal consists of PbI_6 octahedrals, which are tilted with respect to the cubic phase. Bader charge analysis shows that while Cs and Pb atoms donate 0.78 and 0.81 *e*, respectively, and each I atom receives 0.53 *e*.

In order to figure out the thickness dependent characteristics, we first examine bilayer structures derived from truncated bulk orthorhombic $CsPbI_3$. Therefore, two different bilayer configurations were derived from bulk material according to atom types forming the surface of the material. Obtained bilayer structures of Cs−I and Pb−I, shown in Fig. 1 (b), can be given by the chemical formula $Cs_3Pb_2I_7$ and $Cs_2Pb_3I_8$, respectively. Structural analysis reveals that optimized lattice parameters of bilayer $Cs_3Pb_2I_7$ are $a = 7.62$ Å and $b = 9.16$ Å. The thickness of the bilayer $Cs_3Pb_2I_7$ is calculated to be 12.46 Å. As given in Table 1, surface atoms receive 0.6 *e* charge and inner I atoms receive 0.5 *e* charge. In response to this, Pb and Cs atoms donate 0.75 and 0.78 *e* charge. Furthermore, the cohesive energy per atom of bilayer $Cs_3Pb_2I_7$ is found to be 3.13 eV is slightly smaller than that of the bulk structure (3.40 eV).

We complete the thickness-dependent structural analysis via scrutinizing the characteristics of the single layer form of the cesium lead iodide perovskite. As shown in Fig. 2 (c), there exist three possible structures when the material is thinned down to monolayer form. Depending on the atomic compositions, these monolayers can be presented by chemical formulas; $CsPb_2I_5$, $CsPbI_4$, and Cs_2PbI_4. It is calculated that the optimized lattice parameters of monolayer Cs_2PbI_4 are $a = 7.38$ Å and $b = 9.28$ Å. Apparently, reduction of the thickness of the material leads to decrease in the *a* lattice parameter and increase in the b lattice parameter. However, the thickness of the monolayer Cs_2PbI_4 is found to be 6.30 Å. Bader charge analysis reveals that each Cs and Pb atom donates 0.79 and 0.75 *e* charge to surface and inner I atoms that receive 0.64 and 0.52 *e* charges, respectively. Following the trend that surface energy is increased by decreasing thickness, cohesive energy per atom of the monolayer Cs_2PbI_4 is reduced to 3.08 eV.

For understanding the vibrational properties and examination of the dynamical stability of $CsPbI_3$ phonon band dispersions of $CsPbI_3$, $Cs_3Pb_2I_7$, $Cs_2Pb_3I_8$, $CsPb_2I_5$, $CsPbI_4$, and Cs_2PbI_4 are calculated (see in Fig. 2). Here small displacement methodology implemented in the PHONOPY code is used for the determination of elements of dynamical matrix and corresponding phonon spectrum [53]. The phonon spectra of the bulk $CsPbI_3$ crystal exhibits real eigenvalues through all the symmetry points, confirming the dynamical stability of the structure and the reliability of the computational methodology.

It is seen from Fig. 2 that among the possible bilayers of orthorhombic $CsPbI_3$, while the phonon spectrum of $Cs_3Pb_2I_7$ exhibits real eigenvalues through all the symmetry points, that of $Cs_2Pb_3I_8$ possesses imaginary eigenvalues in the large portion between the Γ and S high symmetry points. Therefore, it can be deduced that when the material is thinned down to its bilayers, only $Cs_3Pb_2I_7$ form is expected to be a stable.

Moreover, according to the phonon calculations, among the thinnest possible structures of orthorhombic $CsPbI_3$, although single layer $CsPb_2I_5$ and $CsPbI_4$ have a structure that is obtained by total energy optimization calculations, they cannot form dynamically stable crystal structures.

On the other hand, Cs-rich form given by the formula Cs_2PbI_4 appears as the thinnest stable orthorhombic Cs perovskite. As seen from Table 1, when going from bulk to single layers, cohesive energy decreases while the workfunction increases to 4.68 eV.

4. Electronic and optical properties of ultra-thin $CsPbI_3$

To reveal the effect of dimensional reduction on the electronic properties of $CsPbI_3$ perovskite nanocrystals, electronic band dispersion calculations (by using LDA + PBE0+SOC) are performed.

As shown in Fig. 3 (a), bulk $CsPbI_3$ is a semiconductor with a direct band gap of 1.9 eV. Both the conduction band minimum (CBM) and the valence band maximum (VBM) of the crystal reside at the Γ point. As seen in the previous work [43], contribution of the Cs atom in the material is negligible around the band edges. However, the VBM and CBM of the material are dominated by I-*p* and Pb-*p* orbitals. Fig. 3 (b) shows the electronic band dispersion for stable bilayer structure, $Cs_3Pb_2I_7$. Despite the thinning of the material and the presence of unbonded atoms on the surface, it is seen that the material still exhibits a direct bandgap at the Γ point. Table 1 gives that as the thickness of the crystal decreases to bilayer form, the bandgap of the structure (2.6 eV) is almost 1.5 times of the bulk form (1.9 eV). It is also seen from Fig. 3 (c) that further decrease in dimension leads the significant increase in electronic energy band gap. Single layer Cs_2PbI_4 has a direct bandgap of 2.9 eV at the Γ point. Apparently, while the electronic dispersion characteristics remain unchanged with reduced thickness, the width of the bandgap is significantly enlarged.

Therefore, one can also expect dramatical modifications in the optical properties of $CsPbI_3$ upon dimensional reduction. It is mostly known that decreasing the dimensionality of a semiconductor causes to decreasing of the Coulomb screening. Due to the weakly screened Coulomb interaction between electron and hole, the exciton binding energy of 2D materials increases [54–56]. Sanchez et al. revealed that high exciton binding energy (0.55 eV) has a significant effect on optoelectronic properties of monolayer $CsPbI_3$ [57]. However, in order to avoid the computational burden caused by the large of the number of atoms in the layers, we do not include excitonic effects in our calculations. As represented in Fig. 3(g–j) frequency dependent imaginary dielectric function, absorption coefficient, reflectivity, and transmissivity of bulk, bilayer, and monolayer structures are calculated. The imaginary part of dielectric functions reveals that bulk, bilayer and monolayer $CsPbI_3$ display onset around 1.86, 2.53, and 2.85 eV, respectively. In addition, absorption spectrum shows that first prominent absorption peaks of bulk, bilayer and monolayer orthorhombic $CsPbI_3$ locate around 657, 486, and 431 nm, respectively, indicating a significant blue shift driven by dimensional reduction. As seen in Fig. 3 (i), the reflectivity increases gradually once the layer number increases, reaching a maximum of 30% for bulk. Regardless of the thickness of the material, the most significant peak of reflectivity around the visible range located in between 400 and 450 nm.

Table 1
The calculated parameters for the unit cells of the bulk, bilayer and monolayer $CsPbI_3$; the lattice constants *a,b,c*; layer thickness, *h*; the cohesive energy per atom, E_{Coh}; the amount of electron donated by the Cs, Pb and received by the I atoms are $\Delta\rho_{Cs}$, $\Delta\rho_{Pb}$, and $\Delta\rho_I$, respectively; the band gap of the structures with LDA and PBE0, E_{gap} and E_{gap}^{PBE0} ; the workfunction, Φ.

	A (Å)	*B* (Å)	*C* (Å)	*H* (Å)	E_{Coh} (eV)	$\Delta\rho_{Cs}$ (*e*)	$\Delta\rho_{Pb}$ (*e*)	$\Delta\rho_I$ (*e*)	E_{gap} (eV)	E_{gap}^{PBE0} (eV)	Φ (eV)
Bulk ($CsPbI_3$)	7.93	8.94	12.21	–	3.40	0.78	0.81	0.53	0.66	1.89	–
Bilayer ($Cs_3Pb_2I_7$)	7.62	9.16	–	12.46	3.13	0.78	0.75	0.55	1.26	2.58	4.52
Monolayer (Cs_2PbI_4)	7.38	9.28	–	6.30	3.08	0.79	0.75	0.58	1.55	2.95	4.68

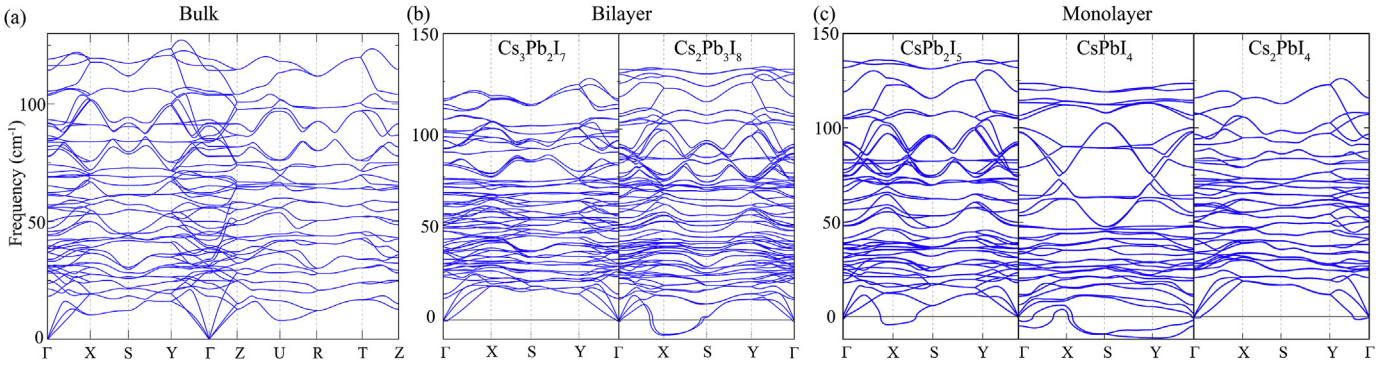

Fig. 2. Phonon band diagram of (a) bulk $CsPbI_3$ crystal in orthorhombic phase, (b) $Cs_3Pb_2I_7$ and $Cs_2Pb_3I_8$ bilayers, (c) $CsPb_2I_5$, $CsPbI_4$, and Cs_2PbI_4 monolayers.

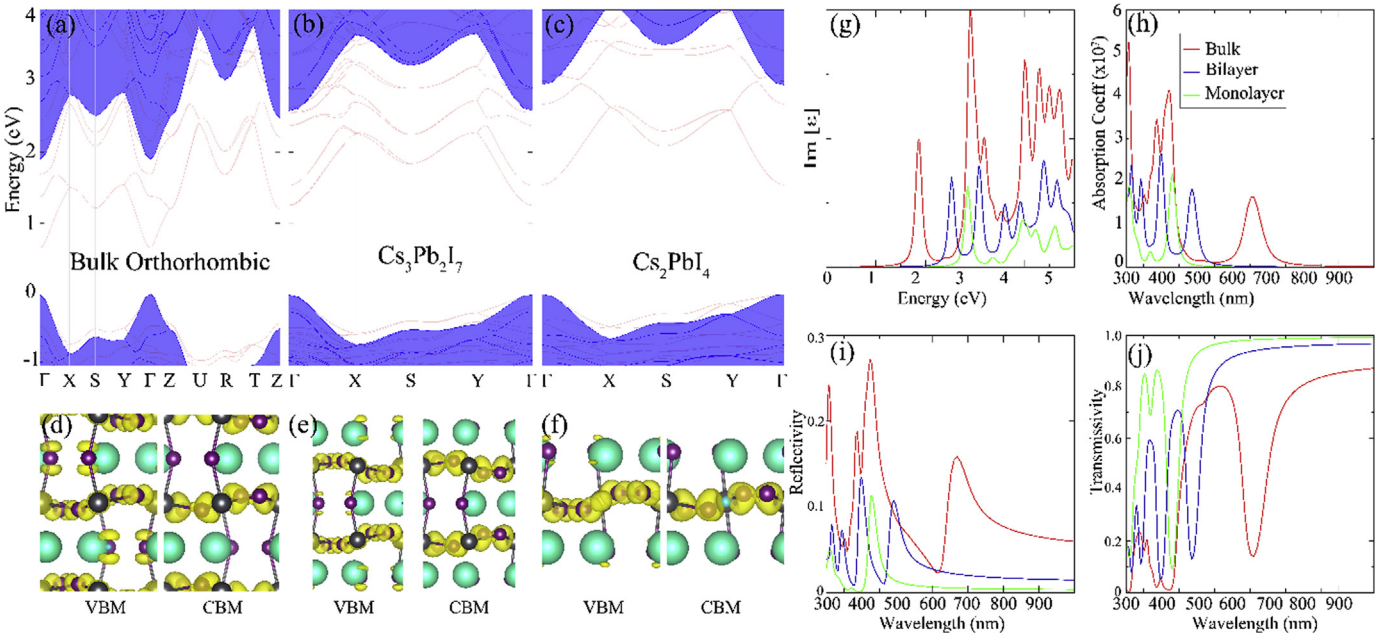

Fig. 3. Electronic band dispersions of (a) bulk, (b) bilayer, (c) monolayer structures of orthorhombic $CsPbI_3$ crystal. VBM and CBM charge densities of (d) bulk, (e) bilayer, (f) monolayer structures of orthorhombic $CsPbI_3$ crystal. The thickness dependent optical properties of CsPbI3 (g) Imaginary part of dielectric function, (h) absorption coefficient, (i) reflectivity, and (j) transmissivity.

Moreover, as illustrated in Fig. 3 (j), as the number of the layer increases the transmissivity of the material decreases. It is seen that while the transmissivity of monolayer and bilayer $CsPbI_3$ is very high in the 600–1000 nm region, that of bulk and bilayer is almost zero near the 400 nm.

5. Enhanced stability via encapsulation

One of the most important issue of perovskite materials are their instability. To the best of our knowledge, the most stable solar cell based on the perovskite has a one-year of lifetime [58]. In addition, as a method to enhance the stability, encapsulation is reported earlier as providing both light and water resistance [59]. In addition, it was reported that the encapsulation of $CH_3NH_3PbI_3$ perovskite by monolayer graphene dramatically enhance the stability of the material and maintain the optical properties upon exposure to moisture and high temperature [60]. Regarding the possible encapsulating materials for the thinnest orthorhombic structure, recently synthesized SnS_2 [61] has quite matching lattice parameters.

In order to examine the stability of the SnS_2-encapsulated monolayers we performed three different sets of molecular dynamic (MD) calculations. In order to construct the heterostructure, we put $1 \times 2 \times 1$ supercell of monolayer $CsPbI_3$ in between two layers of $2 \times 3 \times 1$ rectangular supercells of 1T SnS_2.

In the first set the temperature of the system is kept at 300 K for 5 ps with a time step of 1 fs. In the second and third sets the temperature is increased from 0 to 500 K up to 2 ps and 5 ps with a time step of 1 fs, respectively. The side view geometric structures of all the three cases at the beginning and end of the MD simulations are shown in Fig. 4. It is clear that, as the material is heated, the perovskite exhibits small distortions, while the SnS_2 layers remain quite robust. No geometric reconstructions or broken bonds occur in SnS_2 with increasing temperature. However, the Cs atoms of the perovskite are highly mobile. Fortunately, the SnS_2 layers interact strongly with perovskite and prevent the perovskite from breaking down up to 500 K. Moreover, the SnS_2 layer not only prevents the material from being disassembled up with increasing temperature increases, but also protects the material against environmental factors such as moisture, oxidation and impurities.

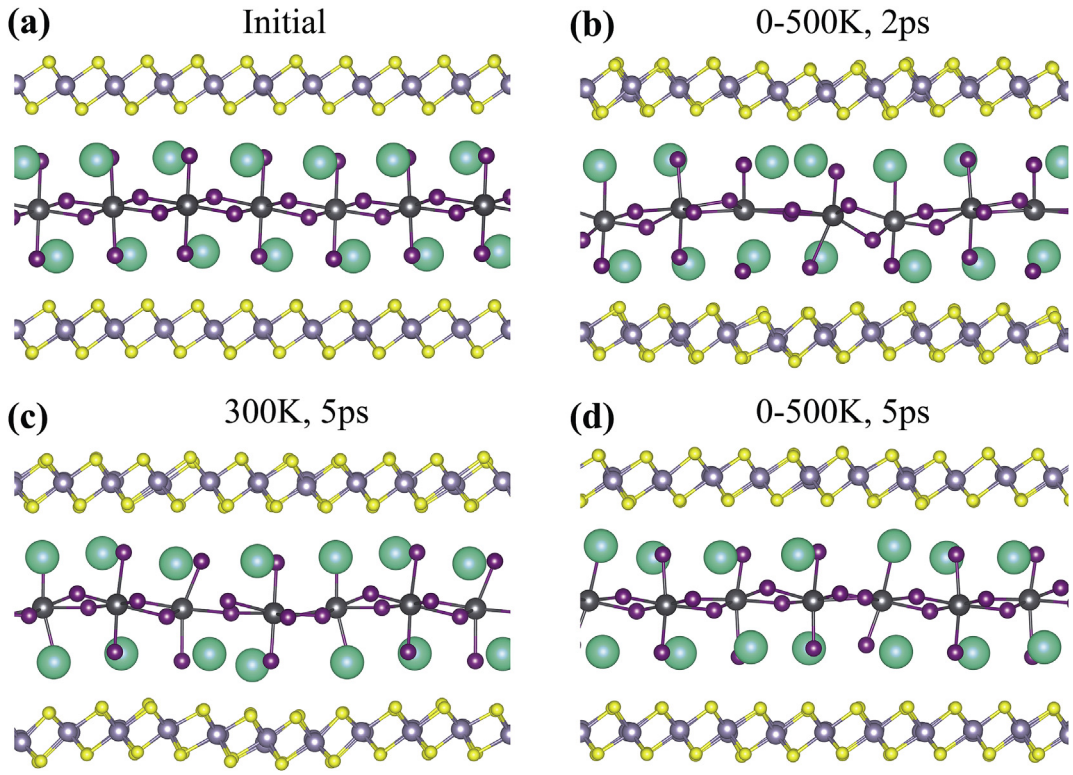

Fig. 4. Molecular dynamics simulations of Cs2 PbI4 monolayer (a) initial configuration, (b) from 0 to 500 K for 2 ps, (c) at 300 K for 5 ps, (d) from 0 to 500 K for 5 ps.

6. Conclusions

In conclusion, based on state-of-the-art first-principles calculations, we investigated thickness dependency of characteristic properties of the orthorhombic phase of $CsPbI_3$ perovskite. Total energy and phonon calculations revealed that only bilayers and monolayers with Cs—I terminated surfaces may form stable thin structures. Electronic structure analysis showed that independent from the thickness all bulk, bilayer and thinnest monolayer forms of orthorhombic phase are direct bandgap semiconductors with valence and conduction band edges located at the Γ symmetry point. However, as the thickness of the perovskite decreases from bulk to bilayer and then monolayer, energy bandgap significantly increases. Moreover, our calculations on the optical response of the structures (dielectric function, absorption coefficient, reflectivity, and transmissivity) showed that reduction in thickness also leads to the blue shift of the absorption edge of the optical spectra. Finally, by performing molecular dynamics calculations, we predicted that even the atomic structure of the thinnest orthorhombic perovskite layer can be well-protected up to 500 K by encapsulating materials such as SnS_2 monolayers. Orthorhombic $CsPbI_3$ perovskites, with their thickness-tunable electronic and optical properties and easy-protected atomic structure, are quite suitable candidates for future optoelectronic applications.

Declaration of competing interest

The authors declare that they have no known competing financial interests or personal relationships that could have appeared to influence the work reported in this paper.

Acknowledgments

Computational resources were provided by TUBITAK ULAKBIM, High Performance and Grid Computing Center (TR-Grid e-Infrastructure). HS acknowledges financial support from the TUBITAK under the project number 117F095.

References

[1] L. Protesescu, S. Yakunin, M.I. Bodnarchuk, F. Krieg, R. Caputo, C.H. Hendon, R.X. Yang, A. Walsh, M.V. Kovalenko, Nano Lett. 15 (2015) 3692.
[2] J. Song, J. Li, X. Li, L. Xu, Y. Dong, H. Zeng, Adv. Mater. 27 (2015) 7162.
[3] T. Guner, M.M. Demir, Phys. Status Solidi A 215 (2018) 1800120.
[4] X. Li, F. Cao, D. Yu, J. Chen, Z. Sun, Y. Shen, Y. Zhu, L. Wang, Y. Wei, Y. Wu, H. Zeng, Small 13 (2017) 1603996.
[5] X. He, Y. Qiu, S. Yang, Adv. Mater. 29 (2017) 1700775.
[6] H. Huang, L. Polavarapu, J.A. Sichert, A.S. Susha, A.S. Urban, A.L. Rogach, NPG Asia Mater. 8 (2016) e328.
[7] M.V. Kovalenko, L. Protesescu, M.I. Bodnarchuk, Science 358 (2017) 745.
[8] G. Nedelcu, L. Protesescu, S. Yakunin, M.I. Bodnarchuk, M.J. Grotevent, M.V. Kovalenko, Nano Lett. 15 (2015) 5635.
[9] S. Ozen, T. Guner, G. Topcu, M. Ozcan, M.M. Demir, H. Sahin, J. Appl. Phys. 125 (2019) 225705.
[10] A.K. Guria, S.K. Dutta, S.D. Adhikari, N. Pradhan, ACS Energy Lett. 2 (2017) 1014.
[11] L.N. Quan, M. Yuan, R. Comin, O. Voznyy, E.M. Beauregard, S. Hoogland, A. Buin, A.R. Kirmani, K. Zhao, A. Amassian, others, J. Am. Chem. Soc. 138 (2016) 2649.
[12] L.-J. Xu, M. Worku, Q. He, H. Lin, C. Zhou, B. Chen, X. Lin, Y. Xin, B. Ma, J. Phys. Chem. Lett. 10 (2019) 5836.
[13] M. Ozcan, S. Ozen, G. Topcu, M.M. Demir, H. Sahin, ACS Appl. Nano Mater. 2 (2019) 5149.
[14] H. Zhu, Y. Fu, F. Meng, X. Wu, Z. Gong, Q. Ding, M.V. Gustafsson, M.T. Trinh, S. Jin, X.-Y. Zhu, Nat. Mater. 14 (2015) 636.
[15] W. Zhang, L. Peng, J. Liu, A. Tang, J.-S. Hu, J. Yao, Y.S. Zhao, Adv. Mater. 28 (2016) 4040.
[16] M. Saliba, T. Matsui, K. Domanski, J.-Y. Seo, A. Ummadisingu, S.M. Zakeeruddin, J.-P. Correa-Baena, W.R. Tress, A. Abate, A. Hagfeldt, M. Gratzel, Science 354 (2016) 206.
[17] M.A. Green, A. Ho-Baillie, H.J. Snaith, Nat. Photonics 8 (2014) 506.
[18] J. Byun, H. Cho, C. Wolf, M. Jang, A. Sadhanala, R.H. Friend, H. Yang, T.-W. Lee, Adv. Mater. 28 (2016) 7515.
[19] L. Zhang, X. Yang, Q. Jiang, P. Wang, Z. Yin, X. Zhang, H. Tan, Y.M. Yang, M. Wei, B.R. Sutherland, E.H. Sargent, J. You, Nat. Commun. 8 (2017) 15640.
[20] P. Wang, X. Bai, C. Sun, X. Zhang, T. Zhang, Y. Zhang, Appl. Phys. Lett. 109 (2016), 063106.

[21] L. Dou, Y.M. Yang, J. You, Z. Hong, W.-H. Chang, G. Li, Y. Yang, Nat. Commun. 5 (2014) 5404.
[22] M.I. Saidaminov, V. Adinol, R. Comin, A.L. Abdelhady, W. Peng, I. Dursun, M. Yuan, S. Hoogland, E.H. Sargent, O.M. Bakr, Nat. Commun. 6 (2015) 8724.
[23] K.S. Novoselov, A.K. Geim, S.V. Morozov, D. Jiang, Y. Zhang, S.V. Dubonos, I.V. Grigorieva, A.A. Firsov, Science 306 (2004) 666.
[24] W.-Q. Han, L. Wu, Y. Zhu, K. Watanabe, T. Taniguchi, Appl. Phys. Lett. 93 (2008) 223103.
[25] B. Radisavljevic, A. Radenovic, J. Brivio, V. Giacometti, A. Kis, Nat. Nanotechnol. 6 (2011) 147.
[26] A.H.C. Neto, K. Novoselov, Rep. Prog. Phys. 74 (2011), 082501.
[27] K.F. Mak, C. Lee, J. Hone, J. Shan, T.F. Heinz, Phys. Rev. Lett. 105 (2010) 136805.
[28] A. Splendiani, L. Sun, Y. Zhang, T. Li, J. Kim, C.-Y. Chim, G. Galli, F. Wang, Nano Lett. 10 (2010) 1271.
[29] Q.H. Wang, K. Kalantar-Zadeh, A. Kis, J.N. Coleman, M.S. Strano, Nat. Nanotechnol. 7 (2012) 699.
[30] Y. Aierken, H. Sahin, F. Iyikanat, S. Horzum, A. Suslu, B. Chen, R.T. Senger, S. Tongay, F.M. Peeters, Phys. Rev. B 91 (2015) 245413.
[31] J.A. Sichert, Y. Tong, N. Mutz, M. Vollmer, S. Fischer, K.Z. Milowska, R.G. Cortadella, B. Nickel, C. Cardenas-Daw, J.K. Stolarczyk, A.S. Urban, J. Feldmann, Nano Lett. 15 (2015) 6521.
[32] P. Tyagi, S.M. Arveson, W.A. Tisdale, J. Phys. Chem. Lett. 6 (2015) 1911.
[33] L. Dou, A.B. Wong, Y. Yu, M. Lai, N. Kornienko, S.W. Eaton, A. Fu, C.G. Bischak, J. Ma, T. Ding, N.S. Ginsberg, L.-W. Wang, A.P. Alivisatos, P. Yang, Science 349 (2015) 1518.
[34] Y. Hassan, Y. Song, R.D. Pensack, A.I. Abdelrahman, Y. Kobayashi, M.A. Winnik, G.D. Scholes, Adv. Mater. 28 (2016) 566.
[35] R.J. Sutton, G.E. Eperon, L. Miranda, E.S. Parrott, B.A. Kamino, J.B. Patel, M.T. Hörantner, M.B. Johnston, A.A. Haghighirad, D.T. Moore, H.J. Snaith, Adv. Energy Mater. 6 (2016) 1502458.
[36] M. Kulbak, D. Cahen, G. Hodes, J. Phys. Chem. Lett. 6 (2015) 2452.
[37] S. Dastidar, C.J. Hawley, A.D. Dillon, A.D. Gutierrez-Perez, J.E. Spanier, A.T. Fafarman, J. Phys. Chem. Lett. 8 (2017) 1278.
[38] G.E. Eperon, G.M. Paternò, R.J. Sutton, A. Zampetti, A.A. Haghighirad, F. Cacialli, H.J. Snaith, J. Mater. Chem. 3 (2015) 19688.
[39] C.M. Guvenc, Y. Yalcinkaya, S. Ozen, H. Sahin, M.M. Demir, J. Phys. Chem. C 123 (2019) 24865.
[40] X. Ding, M. Cai, X. Liu, Y. Ding, X. Liu, Y. Wu, T. Hayat, A. Alsaedi, S. Dai, ACS Appl. Mater. Interfaces 11 (2019) 37720.
[41] G. Shweta, V. Kanchana, Phys. Rev. B 86 (2012) 115209.
[42] G. Shweta, V. Kanchana, G. Vaitheeswaran, J. Solid State Chem. 227 (2015) 110.
[43] F. Iyikanat, E. Sari, H. Sahin, Phys. Rev. B 96 (2017) 155442.
[44] A. Molina-Sánchez, ACS Appl. Energy Mater. 1 (2018) 6361.
[45] G. Kresse, D. Joubert, Phys. Rev. B 59 (1999) 1758.
[46] P.E. Blöchl, Phys. Rev. B 50 (1994) 17953.
[47] G. Kresse, J. Hafner, Phys. Rev. B 47 (1993) 558.
[48] G. Kresse, J. Furthmüller, Phys. Rev. B 54 (1996) 11169.
[49] D.M. Ceperley, B. Alder, Phys. Rev. Lett. B 45 (1980) 556.
[50] G. Henkelman, A. Arnaldsson, H. Jónsson, Comput. Mater. Sci. 36 (2006) 354.
[51] A. Marronnier, G. Roma, S. Boyer-Richard, L. Pedesseau, J.-M. Jancu, Y. Bonnassieux, C. Katan, C.C. Stoumpos, M.G. Kanatzidis, J. Even, ACS Nano 12 (2018) 3477.
[52] R.J. Sutton, M.R. Filip, A.A. Haghighirad, N. Sakai, B. Wenger, F. Giustino, H.J. Snaith, ACS Energy Lett. 3 (2018) 1787.
[53] A. Togo, F. Oba, I. Tanaka, Phys. Rev. B 78 (2008) 134106.
[54] Z. Ye, T. Cao, K. OBrien, H. Zhu, X. Yin, Y. Wang, S.G. Louie, X. Zhang, Nature (London) 513 (2014) 214.
[55] F. Iyikanat, E. Torun, R.T. Senger, H. Sahin, Phys. Rev. B 100 (2019) 125423.
[56] G. Luo, X. Qian, H. Liu, R. Qin, J. Zhou, L. Li, Z. Gao, E. Wang, W.-N. Mei, J. Lu, Y. Li, S. Nagase, Phys. Rev. B 84 (2011), 075439.
[57] A.M. Sánchez, ACS Appl. Energy Mater. 1 (2018) 6361.
[58] G. Grancini, C. Roldán-Carmona, I. Zimmermann, E. Mosconi, X. Lee, D. Martineau, S. Narbey, F. Oswald, F.D. Angelis, M. Graetzel, M.K. Nazeeruddin, Nat. Commun. 8 (2017) 15684.
[59] S.N. Raja, Y. Bekenstein, M.A. Koc, S. Fischer, D. Zhang, L. Lin, R.O. Ritchie, P. Yang, A.P. Alivisatos, ACS Appl. Mater. Interfaces 8 (2016) 35523.
[60] Z. Wang, Q. Ou, Y. Zhang, Q. Zhang, H.Y. Hoh, Q. Bao, ACS Appl. Mater. Interfaces 10 (2018) 24258.
[61] G. Su, V.G. Hadjiev, P.E. Loya, J. Zhang, S. Lei, S. Maharjan, P. Dong, P.M. Ajayan, J. Lou, H. Peng, Nano Lett. 15 (2015) 506.